U.S. DEPARTMENT OF THE INTERIOR
U.S. GEOLOGICAL SURVEY

Debris Flows Triggered by the El Niño Rainstorm of February 2-3, 1998, Walpert Ridge and Vicinity, Alameda County, California

Jeffrey A. Coe *and* Jonathan W. Godt
2001

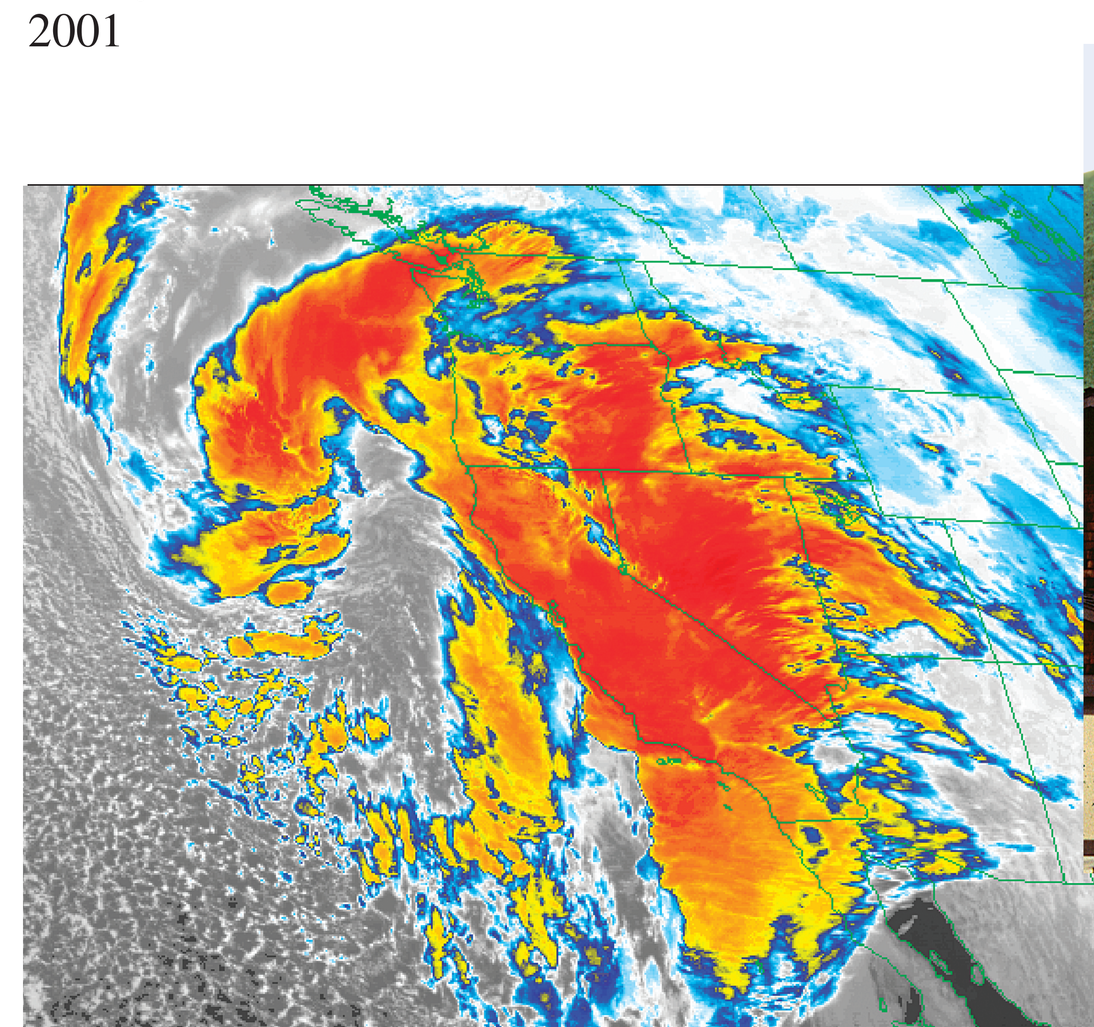

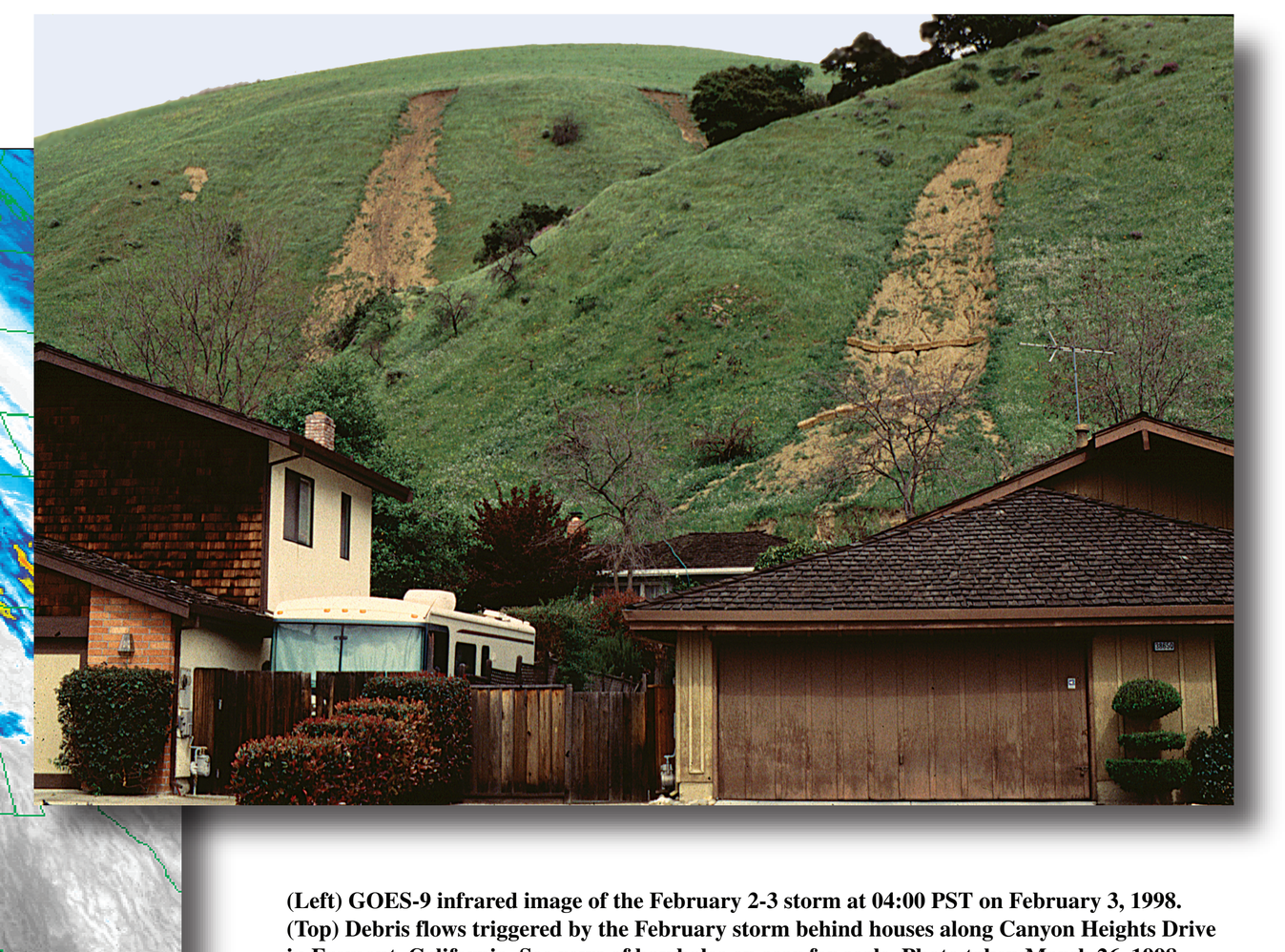

(Left) GOES-9 infrared image of the February 2-3 storm at 04:00 PST on February 3, 1998. (Top) Debris flows triggered by the February storm behind houses along Canyon Heights Drive in Fremont, California. See rows of hay bales on scar for scale. Photo taken March 26, 1998.

ABSTRACT

On February 2 and 3, 1998, a rainstorm generated by the 1997-98 El Niño moved through the San Francisco Bay region of California triggering widespread slope failures. In the Walpert Ridge area of Alameda County, just east of the East Bay cities of Fremont, Union City, and Hayward, 531 debris flows were triggered by the storm. Most of the flows mobilized from soil slips. Maximum concentrations of debris flows reached about 30 per 0.25 km^2. The highest concentrations occurred on west-facing hillslopes well below the crest of Walpert Ridge. Many occurred on the first and second major topographic rises along the western flank of the northwest-trending range front. The highest concentrations occurred on two geologic units having very different physical properties of bedrock and soil mantle, a bedded sedimentary sandstone unit and a rhyolite. Physical property information for each of the 14 geologic units in the study area (mapped at a regional scale) is not sufficient to explain the differences in abundance of debris flows. This disparity indicates that, at least in this part of Alameda County during this rainstorm, geologic materials were not good predictors of debris-flow source areas.

The occurrence of debris flows was controlled primarily by steepness of gradient, topographic curvature that systematically varied as a function of gradient, and the location of moderate to heavy rainfall. Gradients computed from a 10-m digital elevation model at debris-flow initiation locations are approximately normally distributed about a mode of 24∞ Normalizing the debris-flow gradients with the gradients for the entire study area shows that debris-flow incidence increased with gradient. Upslope contributing areas computed from the digital elevation model were less than 10,000 m^2 for 99 percent of the debris flow initiation locations. Debris flows were initiated from both convergent (44%) and divergent source areas (56%) but data indicate that as gradient increased, debris-flow source areas tended to become more divergent. Travel distances were generally between 10 and 200 m.

NEXRAD data indicate that total rainfall from the storm in the study area ranged from about 38 to 139 mm with a maximum 1-hour intensity of about 20 mm/hour. Documented times of debris flow occurrence and end times for maximum rainfall of 1-, 6-, 12-, 18-, and 24-hour durations (as measured by rain gages) all occur within a 12-hour period between 22:00 Pacific Standard Time on February 2 and 10:00 PST on February 3. The close correspondence in end times resulted from a long period of moderate rainfall followed by about a 6-hour period of intense rainfall. In general, debris-flow concentrations corresponded with high cumulative and hourly rainfall, but there was not an exact correspondence between the highest debris-flow concentrations and the highest rainfall. Rainfall at the highest debris-flow concentration did not exceed previously established rainfall thresholds for the initiation of abundant debris flows in the San Francisco Bay region. A comparison of NEXRAD and gage data indicates that there is no systematic difference between cumulative rainfall and only a very slight tendency for NEXRAD to underestimate hourly rainfall. The overall root mean squared errors for cumulative and hourly rainfall are 25 mm and 6 mm, respectively.

INTRODUCTION

As early as the summer of 1997, the 1997/98 El Niño phenomenon was predicted to be one of the most intense in the past 100 years (Monteverdi and Null, 1997; Leetmaa and Higgins, 1998). In the San Francisco Bay region, above average rainfall associated with the El Niño event was also expected to promote an increase in landslide activity (USGS Report, 1997; Godt and others, 1997). By the fall of 1997, the general public in the region experienced an uneasy anticipation of possible 1997/98 El Niño winter storms and associated flooding and slope failures (Diaz, 1997; Perkins, 1997; Perkins and Whetzel, 1997; Richards, 1997; Rogers, 1997). By the end of January 1998, the region had received more than 170 percent of normal rainfall (Aratani, 1998), but experienced only scattered, and relatively minor, slope-failure activity. The largest storm of the 1997/98 winter season occurred on February 2 and 3, 1998 (National Climatic Data Center, 1998a). This storm affected the entire Bay region (Wilson, 1998) and dropped up to about 150 mm of rain in about 30 hours (fig. 1). Following this storm, slope failure was extensively reported by the news media (for example, Akizuki, 1998; Bailey and others, 1998; Buel, 1998; Tucker, 1998). Limited ground reconnaissance of part of the region by USGS scientists on February 4 identified widespread slope failures, including a large number of debris flows in the hills east of Fremont, Union City, and Hayward in Alameda County (M.E. Reid, and S.D. Ellen, written communs., 1998). Slope failures resulting from the February storm prompted the USGS to mobilize field teams to assess damages and cleanup costs in the region. These assessments took place in March and April 1998.

Costs of slope-failure damage caused by winter rainfall in the region totaled approximately $150,000,000 (Highland and others, 1998; Godt, 1999). Damages in Alameda County alone totaled about $20,000,000 (Coe and others, 1999; Godt and others, 2000). Although damage caused specifically by debris flows was relatively minor in Alameda County (about $400,000), the flows themselves were abundant (Coe and others, 1998).

In March and April of 1998, during ground and air reconnaissance to assess damage in the county, we identified two main areas that experienced debris-flow activity (fig. 2a, Coe and others, 1999). The first area, and the subject of this report, is in the vicinity of Walpert Ridge (fig 2b). This area is bounded by the range front on the west, the city of Hayward on the north, Stoneybrook Canyon on the east, and Highway 680 on the south. The second area is northwest of Castro Valley, in the vicinity of Crow, Eden, and Cull Canyons, and is the subject of a separate report. From interviews conducted with homeowners in these areas, and from subsequent reviews of newspaper articles, the February 2-3 storm was identified as the triggering rainstorm for the debris flows.

The primary purpose of this report is to document the distribution, setting, and characteristics of debris flows triggered by the February 2-3 storm in the Walpert Ridge area. The enclosed 1:24,000-scale map, along with the accompanying discussion of debris flow distribution with respect to geologic materials, gradient, geomorphic setting, and rainfall, provides a partial foundation for development of a debris-flow hazard map for Alameda County.

TERMINOLOGY

In this report, **slope failure** is used as the general term for all types of slope movement. The term **landslide** designates slow-moving earth flows and rotational and translational slides (see Varnes, 1978, and Cruden and Varnes, 1996, for classification of slow-moving landslides). The term **debris flow** designates fast-moving flows of mud, gravel, and organic material that commonly mobilize from landslides (see Pierson and Costa, 1987, for classification of fast-moving flows). In the title, we use the term **debris flow** because about 95 percent of the slope failures that we mapped could be classified as debris flows. We group all other types of failures that were mapped under the term **landslide**. At most of the debris-flow source areas that we visited in the field, we observed that the debris flows were mobilized from shallow, freshly activated (winter of 1998) landslides of the type called **soil slips** (Campbell, 1975; Ellen and Fleming, 1987). Even though these flows originate as landslides, we designated the entire feature, including soil slip, flow path, and deposit, as a **debris flow**.

SETTING

Hillslopes in the study area are moderate to steep (10-60°) and are blanketed by colluvial soil cover. Vegetation is mostly grass but includes some shrubs and deciduous trees. Land use is predominantly rural, but is in transition to residential because of the area's proximity to the urban margin. Mean annual precipitation in the area averages about 460 mm in the valleys and tidal flats, but can be as much as 610 mm along upper flanks of the prominent northwest-trending ridges in the area (Rantz, 1971a and b). The most prominent ridge in the study area is Walpert Ridge; its maximum elevation is about 500 m. The ridge is broken by Niles Canyon, which has been carved over time by southwest-flowing Alameda Creek (fig. 2b).

Much of the relief in the study area is controlled by the presence of multiple, active, oblique-slip faults (Graymer and others, 1996). The largest and most active faults are the Hayward (Lienkaemper and Gorchardt, 1996) and Calaveras (Oppenheimer and others, 1990) faults, which lie just to the west and east of the study area, respectively. Although slope failures triggered by earthquakes along these faults have not been documented, evidence from past earthquakes on other faults in the region (Youd and Hoose, 1978), such as the Loma Prieta earthquake in 1989 (Ward and Page, 1989), suggests that the potential exists for widespread slope failures in the event of a moderate-to-large earthquake during a time of high soil moisture (for example, see Wieczorek and others, 1985).

Quaternary landslides and historic debris flows have been well documented in the study area (Waltz, 1971; Nilsen, 1973; Nilsen and others, 1976; Wieczorek and others, 1988). In the past 20 years, hillslopes in the area have experienced at least scattered debris-flow activity in 1982 (Wieczorek and others, 1988), 1986 (S.D. Ellen, oral commun., 1998), and 1995 (R.C. Wilson, USGS, oral commun., 1998). In addition to the landslides and debris flows documented in this report, a large, deep-seated landslide occurred just south of the study area on March 22, 1998, along the west flank of Mission Peak near Fremont (Rogers, 1998). This landslide was about 1.6 km long by 0.4 km wide and was activated within a mapped, but historically dormant, landslide complex.

METHODS

Mapping

Debris flows were mapped from 1:30,000-scale aerial photographs onto portions of four 1:24,000-scale USGS quadrangles (fig. 2b) using a PG2 photogrammetric plotter. The photographs were taken on March 10, 1998, by the National Aeronautics and Space Administration, thus the debris flows documented by this report occurred prior to this date. The scale of the photography allowed us to accurately identify and map debris-flow features as small as about 1 m. Each debris flow shown on the map includes soil slip, flow path, and deposits. Debris flows were mapped if the features appeared to be fresh, that is, nonvegetated. Once mapped, debris flows were digitized from the quadrangles into an ArcInfo Geographic Information System (GIS).

Although we made no systematic effort to field check the maps, the ground and air reconnaissance of landslides described in the introduction and by Coe and others (1999) served to calibrate our photogrammetric mapping.

Creation of isopleth map

Lines (isopleths) on an isopleth map connect equal values of mapped features, such as rates, ratios, or population densities (Schmid and MacCannel, 1955; Campbell, 1973). In this study, an isopleth map was created to distinguish areas of different debris-flow concentration. To create the map, a grid with 250-m spacing between gridlines was overlain on the 1:24,000-scale map of debris-flows. A count circle covering an area of 0.25 km^2 (250,000 m^2) was placed on each grid node and the number of debris-flow soil slips occurring within the circle were counted and recorded. The recorded values were then contoured using values of 1, 5, 10, 15, 20, 25, and 30 debris flows/0.25 km^2. Although landslides that did not generate debris flows are shown on the maps, they were not counted during creation of the isopleth map.

Determination of gradient and upslope contributing area

A gradient and upslope contributing area was measured for each mapped debris flow using USGS 10-m Digital Elevation Models (DEMs, four total, one for each quad in the study area). Gradient and upslope contributing area at each DEM cell were calculated using SINMAP (v. 1.0e) regional slope stability software (Tarboton, 1997; Pack and others, 1999). SINMAP models flow direction based on triangular facets fit to the corners of a 3 x 3 elevation matrix with the gradient computed for each cell along a side of the triangular facet in the steepest downslope direction. Upslope contributing area for each cell is computed by taking the area of that cell plus the area of all cells that have some fraction of flow draining to the cell of interest. Once gradient and contributing area grids were calculated, the mapped debris flows were digitally overlain on the grids. The gradient and contributing area values of the cell coincident with the upslope end of each debris flow (assumed to be the initiation location) were recorded as the values for that debris flow. Errors associated with this method include those related to gradient determination from DEMs of steep hillslopes (for example, see Bolstad and Stowe, 1994), and those associated with the use of a relatively coarse, 10-m grid to determine local gradient from points that could be as much as 7.1 m (distance from the center point to the corner of a cell) away. Additionally, at least one previous study indicates that as DEM cell size increases, local gradients determined from the DEM become smaller (Zhang and Montgomery, 1994).

Determination of topographic curvature

Indices of topographic curvature are often used to infer the direction and concentration of water flow over a topographic surface and can be used to delineate landforms into geomorphic units such as ridges and channels (Zevenbergen and Thorne, 1987; Dikau, 1989; Moore and others, 1991; Gallant and Wilson, 2000). There are three types of topographic curvature that are commonly used, plan curvature, profile curvature, and total curvature (Gallant and Wilson, 2000). Plan curvature is the curvature of a line formed by the intersection of a horizontal plane and the topographic surface, that is, the curvature of a contour line. Profile curvature is the curvature of a line formed by the intersection of a vertical plane and the topographic surface. Total curvature is the curvature of the topographic surface itself, not the curvature of a line formed by the intersection of the surface and a plane.

In this study, we computed total curvature for each cell in the 10-m DEM using the curvature function in the slope stability model SHALSTAB (Montgomery and Dietrich, 1994; Dietrich and Montgomery, 1998). SHALSTAB computes total curvature (TC) using the equation

$$TC = \frac{2(E_2 + E_4 + E_6 + E_8) + (E_1 + E_3 + E_7 + E_9) - 12E_5}{4b^2},$$

where $E_{1,9}$ are elevations in a 3 x 3 window of DEM cells

E_1 E_2 E_3
E_4 E_5 E_6
E_7 E_8 E_9 ,

E_5 is the elevation of the DEM cell for which total curvature is computed, and *b* is the grid cell size (Dino Bellugi, University of California, Berkeley, Department of Earth and Planetary Science, written commun., 2001). For our data, where elevations and cell size are both given in meters, the units of total curvature are m/m^2 or 1/m. Negative values indicate a topographically divergent surface and positive values indicate a convergent surface. Planar surfaces, and surfaces that have equal measures of divergence in one direction and convergence in another, have a total curvature of 0.

Total topographic curvature has been shown to control the downslope transport of colluvial soils, surface runoff, and shallow, sub-surface flow on colluvial mantled hillslopes (Dietrich and others, 1995). Diffusive processes such as soil creep generally dominate below a critical gradient and where total curvature is divergent (Roering and others, 1999). Materials transported by diffusive processes accumulate in convergent areas. As a result, soils tend to be thicker and more susceptible to the initiation of shallow landslides in convergent areas (Dietrich and others, 1986). Previous studies of debris flows in the San Francisco Bay region indicate that convergent areas, commonly called hollows or swales in the Bay region, are commonly the source areas of debris flows (Reneau and Dietrich, 1987; Ellen and others, 1988, Ellen and others, 1997).

As with gradient and contributing area, after total curvature was computed for each DEM cell, the mapped debris flows were digitally overlain on the grid of curvature cells. The curvature value of the cell under the upslope end of each debris flow was recorded as the curvature for that debris flow. There are several potential problems associated with determining the curvature in this manner. First, the upslope end of each debris flow may not accurately represent the source area as a whole. Second, the 10-m DEM may be too coarse to correctly characterize the fine-scale topography found in many debris-flow source areas.

Determination of travel distance

Travel distances are horizontal map distances and were measured from the upslope end of the soil slip to the distal end of the deposit. These distances were determined in ArcInfo by calculating the total length of a series of straight-line segments bisecting each flow roughly parallel to flow direction. Actual travel distances down slopes through the topography are greater than the horizontal distances recorded.

Compilation and analysis of rainfall data

In an effort to relate times of debris-flow occurrence to rainfall intensities and durations, rainfall data were acquired from two sources: National Weather Service (NWS) radio-telemetered automatic rain gages (ALERT gages; see Wilson, 1997, fig 2b) and Next Generation Weather Radar (NEXRAD).

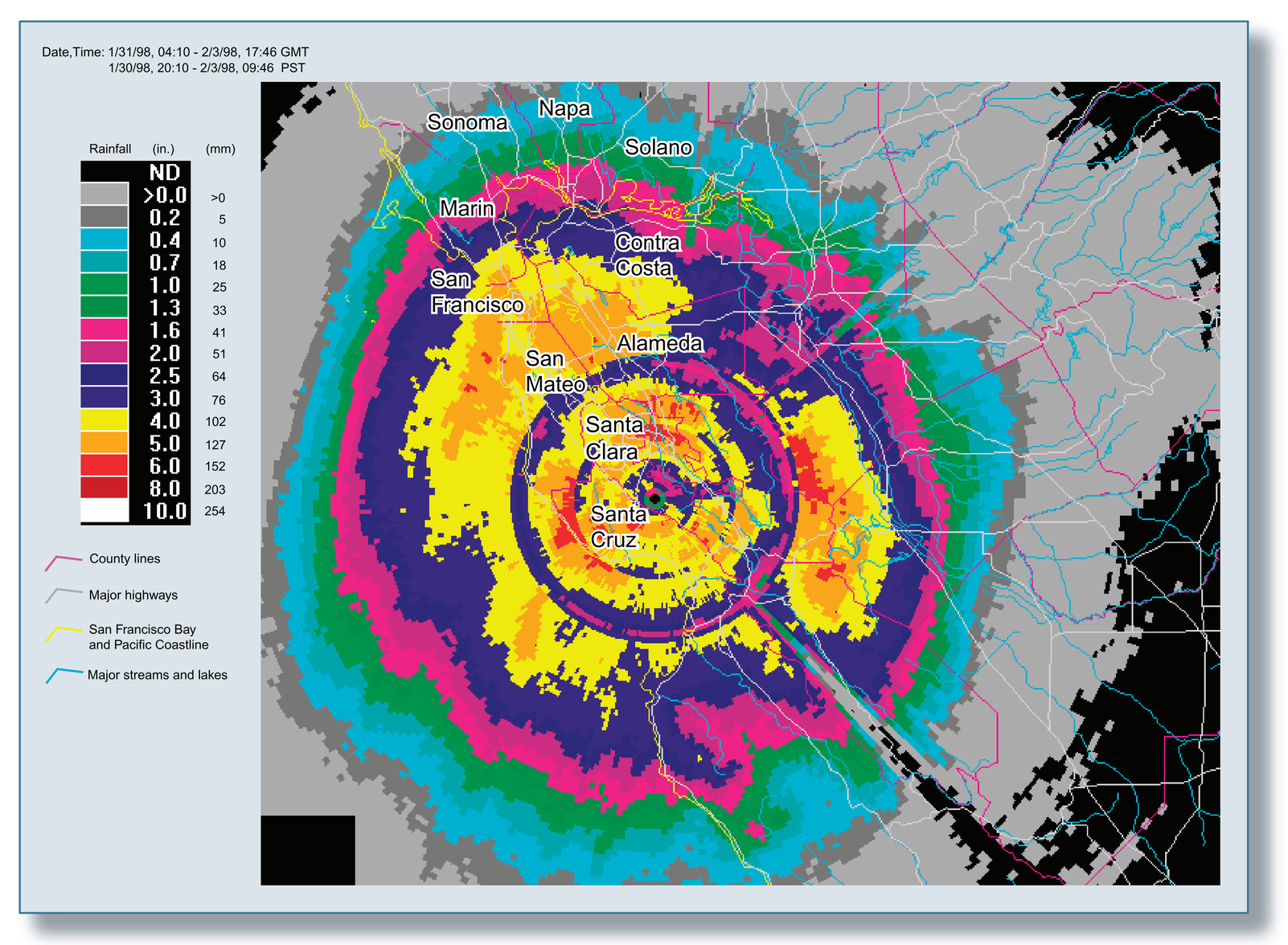

Figure 1. NEXRAD cumulative rainfall in the San Francisco Bay region measured between 20:10 on January 30 and 10:03 on February 3, 1998. Counties bordering San Francisco Bay are labeled. Times are given in Greenwich Mean Time and Pacific Standard Time. Prominent concentric band is described in methods section.

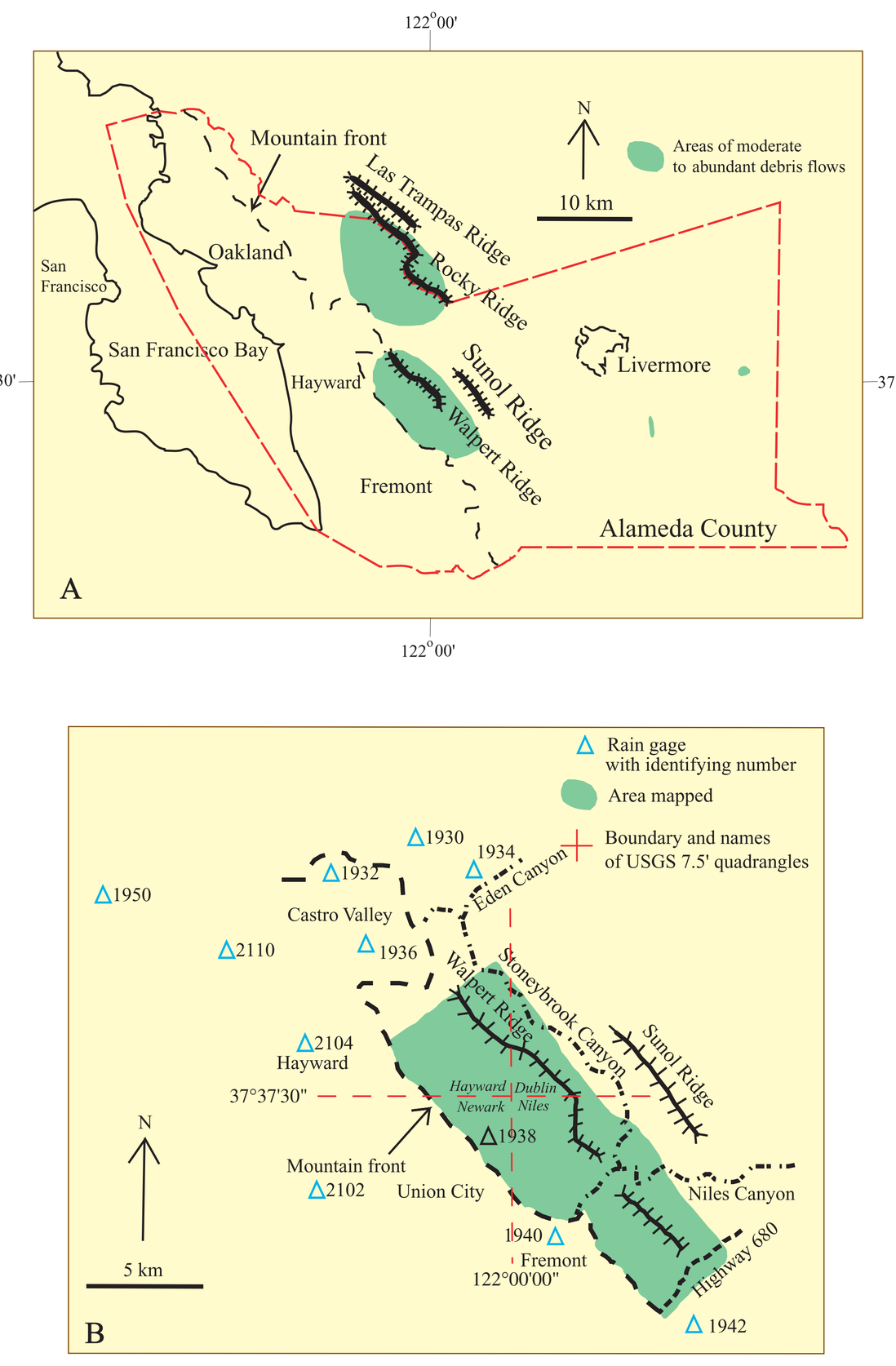

Figure 2. A, Map showing San Francisco Bay, Alameda County, and areas of moderate to abundant debris flows from the February 2-3 storm. B, Map showing the Walpert Ridge study area and rain-gage locations.

Figure 4. Profiles of topography and debris-flow concentration across the study area. Topography shown in black, vertically exaggerated 2x; debris-flow concentration in red. See figure 3 for location of profiles.

Figure 3. Map showing debris flows in the study area. Debris-flow concentrations are shown by isopleths.

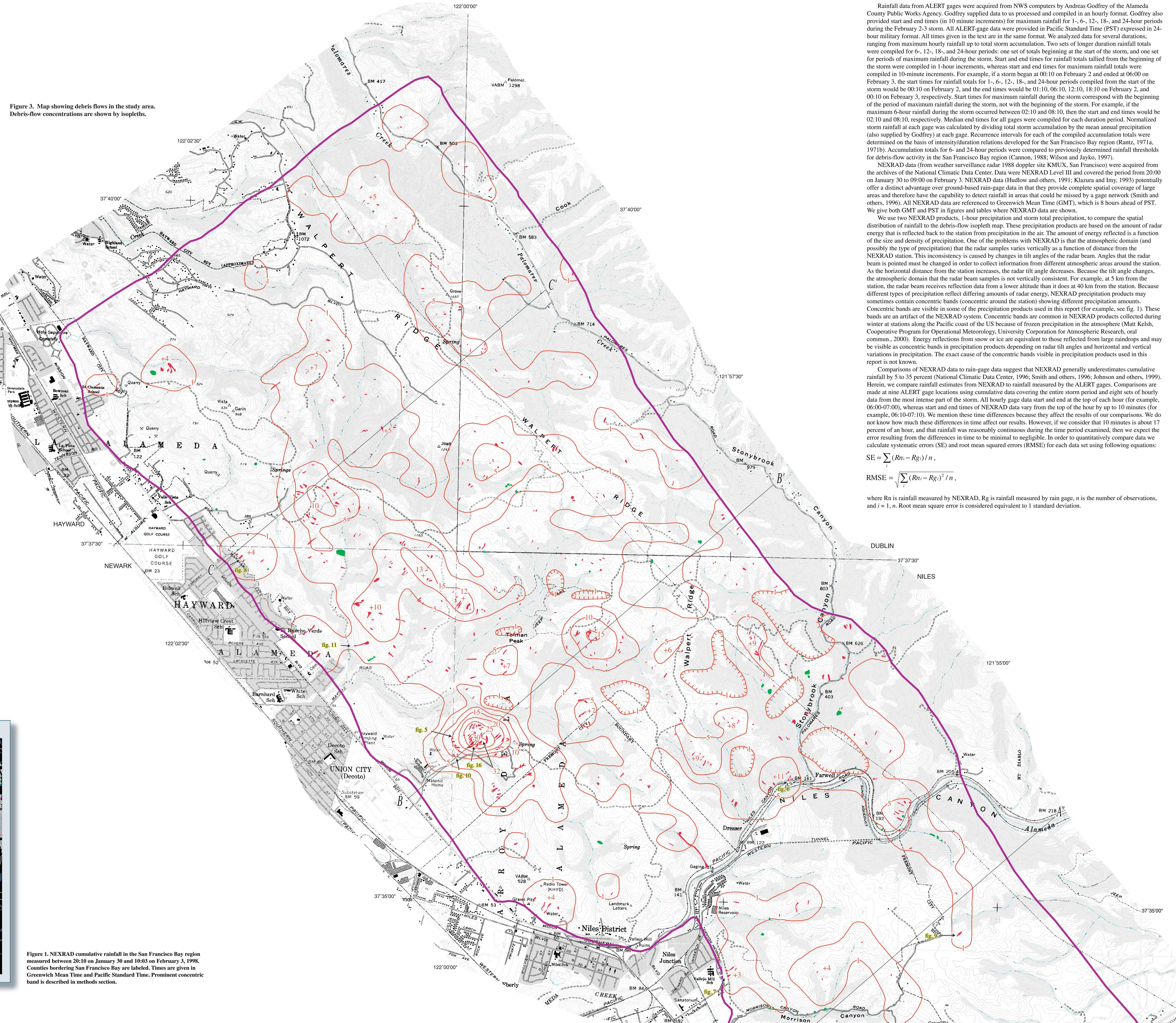

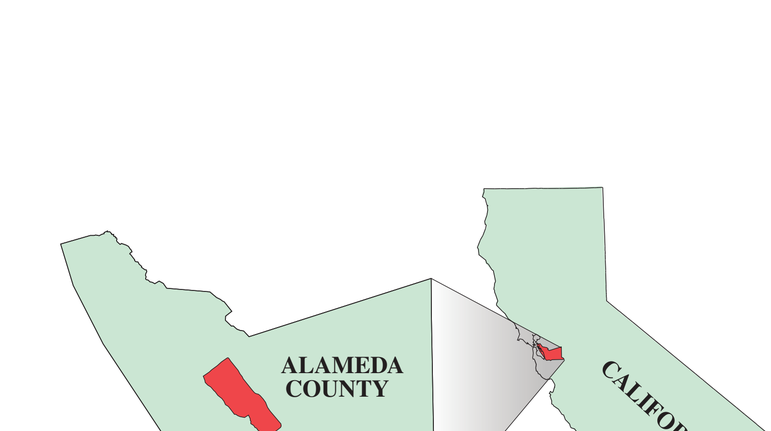

MAP LOCATION

Figure 5. Debris flows located about 1 km northeast of the Masonic Home in Union City. See figure 3 for location and dirt road for scale. Photo taken April 22, 1998.

Rainfall data from ALERT gages were acquired from NWS computers by Andreas Godfrey of the Alameda County Public Works Agency. Godfrey supplied data to us processed and compiled in an hourly format. Godfrey also provided start and end times (in 10 minute increments) for maximum rainfall for 1-, 6-, 12-, 18-, and 24-hour periods during the February 2-3 storm. All ALERT-gage data were provided in Pacific Standard Time (PST) expressed in 24-hour military format. All times given in the text are in the same format. We analyzed data for several durations, ranging from maximum hourly rainfall up to total storm accumulation. Two sets of longer duration rainfall totals were compiled for 6-, 12-, 18-, and 24-hour periods: one set of totals beginning at the start of the storm, and one set for periods of maximum rainfall during the storm. Start and end times for rainfall totals tallied from the beginning of the storm were compiled in 1-hour increments, whereas start and end times for maximum rainfall totals were compiled in 10-minute increments. For example, if a storm began at 00:10 on February 2 and ended at 06:00 on February 3, the start times for rainfall totals for 1-, 6-, 12-, 18-, and 24-hour periods compiled from the start of the storm would be 00:10 on February 2, and the end times would be 01:10, 06:10, 12:10, 18:10 on February 2, and 00:10 on February 3, respectively. Start times for maximum rainfall during the storm correspond with the beginning of the period of maximum rainfall during the storm, not with the beginning of the storm. For example, if the maximum 6-hour rainfall during the storm occurred between 02:10 and 08:10, then the start and end times would be 02:10 and 08:10, respectively. Median end times for all gages were compiled for each duration period. Normalized storm rainfall at each gage was calculated by dividing total storm accumulation by the mean annual precipitation (also supplied by Godfrey) at each gage. Recurrence intervals for each of the compiled accumulation totals were determined on the basis of intensity/duration relations developed for the San Francisco Bay region (Rantz, 1971a, 1971b). Accumulation totals for 6- and 24-hour periods were compared to previously determined rainfall thresholds for debris-flow activity in the San Francisco Bay region (Cannon, 1988; Wilson and Jayko, 1997).

NEXRAD data (from weather surveillance radar 1988 doppler site KMUX, San Francisco) were acquired from the archives of the National Climatic Data Center. Data were NEXRAD Level III and covered the period from 20:00 on January 30 to 09:00 on February 3. NEXRAD data (Hudlow and others, 1991; Klazura and Imy, 1993) potentially offer a distinct advantage over ground-based rain-gage data in that they provide complete spatial coverage of large areas and therefore have the capability to detect rainfall in areas that could be missed by a gage network (Smith and others, 1996). All NEXRAD data are referenced to Greenwich Mean Time (GMT), which is 8 hours ahead of PST. We give both GMT and PST in figures and tables where NEXRAD data are shown.

We use two NEXRAD products, 1-hour precipitation and storm total precipitation, to compare the spatial distribution of rainfall to the debris-flow isopleth map. These precipitation products are based on the amount of radar energy that is reflected back to the station from precipitation in the air. The amount of energy reflected is a function of the size and density of precipitation. One of the problems with NEXRAD is that the atmospheric domain (and possibly the type of precipitation) that the radar samples varies vertically as a function of distance from the NEXRAD station. This inconsistency is caused by changes in tilt angles of the radar beam. Angles that the radar beam is pointed must be changed in order to collect information from different atmospheric areas around the station. As the horizontal distance from the station increases, the radar tilt angle decreases. Because the tilt angle changes, the atmospheric domain that the radar beam samples is not vertically consistent. For example, at 5 km from the station, the radar beam receives reflection data from a lower altitude than it does at 40 km from the station. Because different types of precipitation reflect differing amounts of radar energy, NEXRAD precipitation products may sometimes contain concentric bands (concentric around the station) showing different precipitation amounts. Concentric bands are visible in some of the precipitation products used in this report (for example, see fig. 1). These bands are an artifact of the NEXRAD system. Concentric bands are common in NEXRAD products collected during winter at stations along the Pacific coast of the US because of frozen precipitation in the atmosphere (Matt Kelsh, Cooperative Program for Operational Meteorology, University Corporation for Atmospheric Research, oral commun., 2000). Energy reflections from snow or ice are equivalent to those reflected from large raindrops and may be visible as concentric bands in precipitation products depending on radar tilt angles and horizontal and vertical variations in precipitation. The exact cause of the concentric bands visible in precipitation products used in this report is not known.

Comparisons of NEXRAD data to rain-gage data suggest that NEXRAD generally underestimates cumulative rainfall by 5 to 35 percent (National Climatic Data Center, 1996; Smith and others, 1996; Johnson and others, 1999). Herein, we compare rainfall estimates from NEXRAD to rainfall measured by the ALERT gages. Comparisons are made at nine ALERT gage locations using cumulative data covering the entire storm period and eight sets of hourly data from the most intense part of the storm. All hourly gage data start and end at the top of each hour (for example, 06:00-07:00), whereas start and end times of NEXRAD data vary from the top of the hour by up to 10 minutes (for example, 06:10-07:10). We mention these time differences because they affect the results of our comparisons. We do not know how much these differences in time affect our results. However, if we consider that 10 minutes is about 17 percent of an hour, and that rainfall was reasonably continuous during the time period examined, then we expect the error resulting from the differences in time to be minimal to negligible. In order to quantitatively compare data we calculate systematic errors (SE) and root mean squared errors (RMSE) for each data set using following equations:

$$SE = \sum_i (Rn_i - Rg_i)/n,$$

$$RMSE = \sqrt{\sum_i (Rn_i - Rg_i)^2 / n},$$

where Rn is rainfall measured by NEXRAD, Rg is rainfall measured by rain gage, *n* is the number of observations, and *i* = 1, *n*. Root mean square error is considered equivalent to 1 standard deviation.

RESULTS

Distribution and concentration of debris flows

A total of 531 debris flows were mapped in the 91 km^2 study area (fig. 3 and appendix). About 39 percent of the study area had concentrations equal to or greater than 1 debris flow/0.25 km^2 (table 1). Concentrations of 10 or more debris flows/0.25 km^2 made up only about 1 percent of the map area. The largest number and highest concentrations of debris flows occurred in the central portion of the study area, on the west side of the crest of Walpert Ridge on the first and second major topographic rises of the range front (fig. 3; fig. 4). The highest concentration of debris flows was about 30/0.25 km^2 and occurred as a prominent peak on the isopleth map about 1 km northeast of the Masonic Home in Union City (fig. 3, fig. 5).

Debris flows that caused notable damage occurred in Niles Canyon (fig. 6), near the mouth of Niles Canyon in Fremont (fig. 7), and along the western edge of the range front in Hayward (fig. 8). These damaging debris flows occurred in areas of low to moderate (1 to 5 debris flows/0.25 km^2) concentrations (fig. 3). Interviews with homeowners and maintenance personnel at these damage sites, as well as a review of newspaper articles, revealed the February 2-3 storm as the only possible trigger for recent debris flows in the study area (table 2).

Debris-flow source areas

Although we did not systematically compile information on slope failures in source areas of mapped debris flows, observations from the field and aerial photos suggest that the vast majority of flows were mobilized from soil slips, that is, shallow slides of the colluvial soil cover (Campbell, 1975; Ellen and Fleming, 1987). Scarps at the heads of soil slips were as much as about 30 m wide (fig. 9), but most were between 2 and 15 m wide (frontispiece). In general, soil slips were less than 1.5 m deep, and almost everywhere less than 2 m deep (figs. 8 and 9). In the area of highest concentration, near the Masonic Home, several debris flows were mobilized from soil slips on hillslopes already deformed by terracettes (Selby, 1993; fig. 10). In the Garin Park area, at least one debris flow was mobilized from the toe of an earth flow (fig. 11).

Relation between debris flows and geologic materials

The study area is underlain mostly by Jurassic and Cretaceous sedimentary rocks, and to a less extent by Tertiary sedimentary rocks, serpentinite, altered volcanic rock, and rhyolite (fig. 12; table 3; see Ellen and Wentworth, 1995; Graymer and others, 1996; Wentworth, 1997). Below, we compare the mapped distribution of debris flows to the distribution of geologic materials units and the physical properties of the units. We did not examine the geology in the study area and, therefore, all geologic unit and physical property descriptions referred to herein are from Ellen and Wentworth (1995). About 58 percent of the area is underlain by Cretaceous sandstone and shale of the Great Valley Sequence (unit 644; appendix; fig. 12; table 3). The largest number of debris flows (362, 68% of the total number) originated within the soil mantle formed on this unit (table 4). To gain a sense of susceptibility of these different geologic units, it is useful to normalize the abundance of debris flows in each unit according to the area covered by that unit. As shown in table 4, the number of debris flows/km^2 for unit 644 is 6.8/km^2. The highest number of debris flows/km^2 occur in two units (133 and 215, table 4, fig. 12) that are reported to have very different physical properties of bedrock and soil mantle (table 3). Unit 133 is soft, young interbedded conglomerate, sandstone, and shale with a dominantly clayey, expansive soil mantle of low permeability. Unit 215 is a rhyolite with a granular soil mantle of moderate permeability. Although the area covered and the actual number of debris flows in units 133 and 215 is small (table 4), the number of debris flows/km^2 is high (40.0/km^2 and 13.2/km^2, respectively). The magnitude of these normalized numbers, when compared to other units (see table 4, column 5), suggests that the two units are much more susceptible to debris flows than other units in the area. A relative susceptibility ranking for all of the units created from the number of debris flows/km^2 is shown in table 5. In this ranking, high numbers of debris flows/km^2 (for example, units 133 and 215, table 4) have a high susceptibility ranking (table 5), and small numbers (for example, units 389 and 805) have a low ranking. This ranking, however, makes little sense when the physical properties of the units are examined (table 5). Properties that seemingly would make a unit more or less susceptible, such as permeability, clay content, and expansivity, are not consistently high or low when compared to the susceptibility rankings. One might expect, for example, that a unit with low soil-mantle permeability and moderate bedrock permeability might be more susceptible than a unit with high soil-mantle permeability and low bedrock permeability. Clay content and expansivity data are more difficult to interpret because only a small amount of clay is generally needed to initiate and maintain debris flows; however, there is no consistent pattern to these data that is sufficient to explain the susceptibility ranking. It is unclear, therefore, whether this apparent relative susceptibility ranking is real or that the flows are concentrated on these units simply because rainfall may have been greatest in the area underlain by these units. As shown in figure 12, the high occurrence that is concentrated in dissimilar units (133 and 215) within a small area, combined with low occurrence elsewhere in unit 215 of the study area, suggest that the debris-flow concentrations result from local topographic and rainfall conditions.

Relation between debris flows and gradient

The entire population of gradients at 10-m DEM nodes in the study area ranges from 0 to 60° (appendix; fig. 13). The mode of these gradient values is 15° (fig. 13). The steepest gradients generally occur along the flanks of Niles and Stoneybrook Canyons (unpublished gradient map by Scott Graham, 1998).

About 94 percent of the debris flows initiated on gradients between 10 and 45° as measured from the 10-m DEM (table 4; fig. 13). Gradients on which all 531 debris flows initiated are approximately normally distributed about a mode of 24∞and a mean of 26.2° (fig. 13; table 4). Means of gradients by unit range from about 19 to 28° (table 4). In units 644 and 133, which each have more than 30 debris flows, gradients are also approximately normally distributed.

The approximately normal distribution of gradients at debris-flow initiation locations about a mode of 24° suggests that the incidence of debris flows decreases progressively for gradients shallower and steeper than 24°. Intuition, however, suggests that the tendency for debris flows should increase as gradient increases, providing that geologic materials are available to fail. A possible explanation for this apparent disparity is that the distribution of debris-flow gradients is a reflection of the gradients available. For example, if there were only a few steep gradients in the study area, then only a small number of debris flows could occur on steep gradients. In order to account for the varying availability of gradients, we followed the method of Wieczorek and others (1988) and calculated the ratio of debris-flow initiation gradients to the total population of gradients within the study area (fig. 13). In general, the ratio increases as gradient increases. Wieczorek and others (1988) found that debris-flow incidence in San Mateo County, directly west of Alameda County, peaked between 25∞and 29° (measured using a 30-m DEM) and then dropped off and reached a low point at about 42°. Ellen and others (1988) found a similar pattern in Marin County (measured from spacing of 40 ft contours), with a peak between about 30∞and 36°, and a low point at about 42°. Neither of these studies presented data above 42°. Our data show similar patterns, but overall indicate that incidence increases as gradient increases (up to at least 52∞).

Relation between debris flows and contributing area and topographic curvature

About 99 percent of debris flows were initiated from hillslope locations with upslope contributing areas less than 10,000 m^2 (appendix and fig. 14a). In general, convergent initiation locations had larger upslope contributing areas than divergent locations (fig. 14a). A scatter diagram of the means of contributing areas (calculated for each set of debris-flow initiation locations partitioned by 1∞increments of gradient) plotted as a function of gradient indicates that as gradient increases, contributing areas (on average) remain relatively constant between about 300 and 2,000 m^2 (fig. 14b). These data indicate that large upslope contributing areas are not a requirement for the initiation of debris flows.

Debris flows were initiated in near equal numbers from both convergent and divergent hillslopes, with about 44 percent of debris flow initiation locations in cells that are convergent and 56 percent in cells that are divergent (appendix). A scatter diagram of total curvature plotted as a function of gradient for each debris flow initiation location does not reveal a relation between the two variables (fig. 15a). However, a scatter diagram of the means of curvature values (calculated for each set of debris flows partitioned by 1∞increments of gradient) plotted as a function of gradient indicates that as gradient increases, cells containing debris-flow initiation locations tend to become more divergent (fig. 15b). Figure 15b indicates that on gradients equal or less than about 24∞ debris flows tended to initiate from convergent locations, whereas on gradients greater than 24∞ they tended to initiate from divergent locations. These results do not match results from previous studies in the San Francisco Bay region that suggest most debris flows initiate from convergent locations (Dietrich and others, 1986; Reneau and Dietrich, 1987), but are similar to results from Madison County, Virginia (Wieczorek and others, 1997). One possible reason for the difference in results may be our use of the most upslope location of each debris flow as an initiation location rather than using locations in a more central part of the upper portion of each debris flow. For a visual check on the type of curvature in source areas, we created and inspected a map of curvature overlain with debris flows. This inspection revealed that, although in a few cases use of the most upslope locations skewed our curvature results to be more divergent, many of the debris flows simply initiated from divergent locations. Another possible reason that our results are different from previous studies is that the 10-m DEM used to compute curvature may be inadequate to resolve fine-scale details in topography in debris-flow source areas. For many debris-flow hazard studies, however, a 10-m DEM is the highest resolution DEM available. Our data suggest that, when using a 10-m DEM in debris-flow hazard studies, at least in Alameda County, both convergent and divergent locations need to be recognized and delineated as potential debris-flow source areas.

Debris-flow travel distances and deposits

Distances over which debris flows traveled were short compared to many debris flows elsewhere, with most (about 98%) traveling between 10 and 200 m. The longest travel distance in the study area (643 m) occurred in a drainage on the north side of Niles Canyon near Dresser (fig. 3). Mean travel distances show considerable variability between geologic units. Mean distances range from about 35 m in unit 389 to 81 m in units 616 and 215 (table 4). There is no correlation between travel distances and initiation gradients, which suggests that travel distances are primarily a function of the physical properties of the flows and/or the topography over which the flows travel.

Field and aerial photo observations suggest that all debris flows tended to have very thin deposits along their flow paths. In many places, flow paths consist largely of flattened grass without appreciable material left behind. In the area of highest concentration near the Masonic Home, a comparison of photos taken one day after the event (fig. 16a) to one taken about 2 months later (fig. 16b), shows thin flow deposits that are rendered nearly invisible by rapidly growing vegetation. This comparison suggests that, in as little as 6 months after their occurrence, debris-flow deposits would be undetectable from the air and that travel distances could not be measured remotely or, quite possibly, by ground-based methods.

Antecedent soil moisture

Nine NWS ALERT rain gages recorded rainfall near the study area in the winter of 1997/1998 (fig. 2b, table 6). Mean annual precipitation at these gages ranges from 460 to 685 mm and generally exhibits a positive correlation with gage elevation (table 6).

Cumulative rainfall at ALERT gages for the 1-month period (January 1 to February 1, 1998) prior to the February 2-3 storm ranged from 153 to 264 mm (33 to 46% of the mean annual precipitation, table 6). Previous studies suggest that a minimum of 254-280 mm of pre-storm seasonal rainfall is needed to reach antecedent moisture conditions necessary for the occurrence of debris flows in the San Francisco Bay area (Campbell, 1975; Wieczorek and Sarimiento, 1988). Seasonal rainfall is defined as beginning on October 1 of any given year. Rainfall from October 1 through December 31, 1997, at all long-term National Weather Service gages (non-ALERT gages) near the study area exceeded 200 mm (National Climatic Data Center, 1998b and 1999). When combined with the January 1998 rainfall, these data show that soil-moisture conditions in the study area prior to the February 2-3 storm were well above the antecedent conditions considered necessary for the occurrence of debris flows.

Cumulative rainfall from the February 2-3 storm

The February 2-3 storm lasted approximately 30 hours, from about 05:00 on February 2 to about 10:00 on February 3 (table 6). Although there was a 2-3 hour variability in the start time of the storm at various ALERT gages (table 6), there is no obvious pattern with respect to gage elevation or geographic location, and so no conclusions can be drawn from the start times regarding storm movement. Storm movement can be tracked, however, from a national mosaic of NEXRAD images (National Oceanic and Atmospheric Administration, unpublished data, 1998) acquired during the storm period. These images reveal the counterclockwise flow of the storm and general west-to-east movement through the San Francisco Bay region, which brought the rain into the southwest-facing range front of the study area.

Total storm rainfall measured by ALERT gages near the study area ranged from about 58 to 119 mm (table 6, fig. 1b, fig. 17), and these totals, unlike mean annual precipitation, tended to be inversely correlated with elevation. The ALERT gages closest to the study area are, from south to north, numbers 1942, 1940, 2102, 2104, 1936, and 1934 (fig. 2b). Storm rainfall normalized by mean annual precipitation at these gages ranged from 0.11 at gage 1942 to over 0.23 at gages 2102 and 2104 (table 6). Unfortunately, gage 1938, located within the study area, was malfunctioning during the storm and did not record rainfall.

Within the study area, total rainfall measured by NEXRAD for the period between 20:10 on January 30 and 10:03 on February 3 ranges from about 51 mm to 152 mm (fig. 18). Rain-gage data suggest that less than 13 mm of rain fell between 20:10 on January 30 and the start of the storm on February 2. Therefore, by subtracting 13 mm from the NEXRAD total, NEXRAD indicates that rainfall from the February 2-3 storm in the study area ranged from about 38 mm to 139 mm.

Hourly rainfall during the February 2-3 storm

ALERT gages (fig. 17, table 6) indicate that the maximum hourly rainfall near the study area occurred between 22:00 on February 2 and 01:00 on February 3. Maximum hourly rainfall rates during this time ranged from 11 mm/hour at gage 1950 to 23 mm/hour at gages 2102 and 2110. At gages closest to the study area (1942, 1940, 2102, 2104, and 1936), maximum rates ranged from 17 mm/hour at gage 1936 to 23 mm/hour at gage 2102. Maximum hourly rainfall at four of the nine gages exceeded the amount with a 10-year recurrence interval. Maximum hourly rainfall at gage 1940 exceeded the amount with a 25-year recurrence interval, whereas maximum hourly rainfall at gages 2102 and 2104 exceeded the amount with a 50-year recurrence interval (table 6).

In general, maximum rainfall amounts become more exceptional (for the area as a whole) as the length of observation increases (table 6). For example, for a 6-hour period, maximum rainfall exceeds the amount with a 10-year recurrence interval at five of the nine gages. For 18- and 24-hour periods, maximum rainfall exceeds the amount with a 10-year recurrence interval at seven of the nine gages. The exception to this observation is the 12-hour period, where maximum rainfall at only two gages exceeds the amount with a 10-year recurrence interval. Previously established debris-flow thresholds are exceeded for all time periods only at gages 2102 and 2104 (table 6).

NEXRAD data provide a synoptic view of the storm in hourly increments recorded about every half hour (fig. 19). Figure 19 shows three cells of moderate-to-heavy precipitation moving from west-to-east through Alameda County between the hours of 18:30 on February 2 and 03:30 on February 3. The first two cells pass to the north and south of the study area (fig. 19d-g). The third cell passes directly over the study area between the hours of 23:30 on February 2 and 02:00 on February 3 (fig. 19k-n). Maximum hourly rainfall recorded within the study area was 20 mm and occurred between 01:00 and 02:00 (fig. 19n). NEXRAD data show that the northern half of the study area received more intense and prolonged rainfall than the southern half, although the concentric banding problem described in the methods section, and observed in figure 19, makes this observation somewhat suspect.

Comparison of rainfall measured by ALERT gages and NEXRAD

A qualitative comparison of ALERT gage and NEXRAD data indicates that there is a 2-hour difference in the times of maximum hourly rainfall. Most ALERT gages indicate the time of maximum hourly rainfall *near the study area* was between 23:00 on February 2 and 00:00 on February 3 (table 6). NEXRAD indicates the time of maximum hourly rainfall *within the study area* was between 01:00 and 02:00 on February 3. This discrepancy is probably due to several factors. First, all gages are located outside the study area, whereas NEXRAD data are observations from within the study area. Most of the gages are located to the west and north of the study area. Therefore, with the eastward moving storm, the time of maximum rainfall in the study area would be expected to lag behind that recorded by the gage network. Second, gages sample precipitation at the surface of the earth, whereas NEXRAD samples precipitation in the atmosphere. Precipitation close to the surface of the earth is not represented well by NEXRAD (Matt Kelsh, Cooperative Program for Operational Meteorology, University Corporation for Atmospheric Research, oral commun., 2000). This sampling difference would also be expected to cause a discrepancy in the recorded times of maximum rainfall.

A quantitative comparison between rainfall measured by ALERT gages (fig. 17, table 6) and NEXRAD (figs. 17 and 18) is shown in table 7. The systematic error (SE) and Root Mean Squared Error (RMSE) for cumulative rainfall for the period between 20:00 on January 30 and 10:00 on February 3 are 0 mm and 25 mm, respectively (table 7). The SE of 0 mm indicates that there is no systematic difference between cumulative rainfall measured by gages and NEXRAD. Negative numbers for SEs and individual difference values indicate that rainfall measured by NEXRAD is less than that measured by gages. The RMSE of 25 mm is about 20 percent of the maximum cumulative amount of rain measured by NEXRAD (127 mm at five gages, table 7) and about 16 percent of the maximum cumulative amount of rain measured by gages (156 mm at gage 1932, table 7). The RMSE is about 33 percent of the minimum cumulative amount of rain measured by NEXRAD (76 mm at gages 1940 and 1950) and about 40 percent of the minimum cumulative amount of rain measured by gages (~62 mm at gage 1942). The maximum difference in measured rainfall (40 mm) occurs at gage 1942, which is the gage at the highest elevation. In the concentric banding area that encompasses the southern half of the study area, the difference in rainfall between NEXRAD and gage 1940 is −29 mm.

A comparison of hourly data (table 7) shows differences at individual rain gages that range from −19 to +15 mm. The largest differences for 3 of the 8 hourly data sets occur at gage 1942, located at the highest elevation. The differences at gage 1942 are not consistently negative or positive. At gage 1940, in the concentric banding area, difference values are negative for all hourly data sets and range from −10 to −1. For the entire gage network, systematic errors for individual hours range from −8 mm to +4 mm with 5 of the 8 hourly data sets having negative SEs. The grand SE for all hourly data is −1 mm. Root mean squared errors at individual gages range from 1 to 11 mm. The largest RMSEs (3-11 mm) occur between the hours of 21:00 on February 2 and 02:00 on February 3, which is generally the period of heaviest precipitation. The grand RMSE for all hourly data is 6 mm.

In summary, the 2-hour difference in times of maximum rainfall is probably due to differences in the geographic location of the gages with respect to the NEXRAD data, as well as differences in sampling methods. There is no systematic difference between cumulative rainfall measured by the ALERT gages and NEXRAD. The comparison of hourly data shows there is a very slight tendency for NEXRAD to underestimate rainfall. Overall RMSEs (equivalent to 1 standard deviation) for cumulative and hourly data are 25 mm and 6 mm, respectively. The largest differences in measured rainfall tend to occur during heavy rainfall and at higher elevations. Within the concentric banding in the southern half of the study area, NEXRAD underestimated cumulative rainfall by about 29 mm and hourly rainfall by 1 to 10 mm.

Relation between debris flows and rainfall

About 80 percent of all mapped debris flows are in the northern half of the study area (fig. 3). Gage and NEXRAD data both suggest that the northern half of the study area received more cumulative rainfall than the southern half of the study area. In general, gage data indicate that gages near the northern half of the study area (gages 1932, 1936, 1950, 2102, 2104, and 2110, fig. 17) received up to two times more cumulative rainfall than gages near the southern half (gages 1940 and 1942, fig. 17). NEXRAD data indicate that the northern half of the study area received up to 2.5 times more rain than the southern half (fig. 18), although this estimate includes the bias caused by concentric banding as described in the previous section. If the bias is corrected by adding 29 mm of rainfall to areas with concentric banding, NEXRAD still indicates that the northern half of the study area received up to 1.5 times more rain that the southern half.

In general, debris-flow concentrations in the northern half of the study area correspond with high cumulative and hourly rainfall, but there is not an exact correspondence between the highest debris-flow concentrations and highest cumulative and hourly rainfall (fig. 18; fig. 19k-n). For example, rainfall at the highest debris-flow concentrations east of the Masonic Home in Union City (fig. 3, fig. 5, fig. 16) was relatively high compared to rainfall in the southern half of the study area, but less than rainfall in other parts of the northern half of the study area that had fewer debris flows (fig 17, fig. 19n). This indicates that one or more other variables, in addition to adequate intensity and duration of rainfall, determined the occurrence of debris flows. Previous sections of this report indicate that gradient and topographic curvature are the primary additional variables.

For specific rainfall amounts in the northern half of the area, NEXRAD data are all that is available. According to NEXRAD data, the northern half of the study area received cumulative precipitation between 114 mm and 139 mm during the 30-hour February 2-3 storm (127-152 mm from January 30 to February 3, fig. 18). Hourly NEXRAD data from the peak of the storm show rainfall intensities of 15 to 20 mm/hr between 00:59 and 01:59 on February 3 (fig. 19n). The maximum 6-hour rainfall occurred between 21:00 on February 2 and 03:00 on February 3 (from NEXRAD, fig. 19f-p). At the location of the high debris-flow concentrations near gage 1938, the maximum 6-hour rainfall was 51 mm (figs. 18f-p). Debris flow thresholds have been developed for 6-hour periods, but have not been defined for 30- and 1-hour periods (Cannon, 1988; Wilson and Jayko, 1997). The 6-hour rainfall of 51 mm at gage 1938 does not exceed previously established debris-flow thresholds (compared using a mean annual precipitation of 559 mm from gage 1938).

Documented times of debris-flow occurrence are mostly inexact, but consistently indicate that debris flows occurred within a 12-hour period between about 22:00 on February 2 and 10:00 on February 3 (table 2). The median end times (from gage data) for maximum 1-, 6-, 12-, 18-, and 24-hour rainfall during the storm were 23:50 on February 2, and 02:50, 01:10, 03:00, and 03:00 on February 3, respectively (table 6). The close correspondence in the end times of various durations resulted from the storm pattern, a long period of moderate rainfall followed by about a 6-hour period of intense rainfall (fig. 17). The median end times all fall within a window of time that corresponds with documented times of debris flows (fig. 20). Even considering a possible 2-hour shift between rainfall at the gages and rainfall in the study area (described in previous section) the median end times would still correspond with documented times of debris flows. Although the median end times don't help to identify an intensity/duration trigger, they do indicate that any of the maximum rainfall durations may have been the trigger, or that the debris flows may have been triggered because all of the median end times closely corresponded.

The most accurate time of debris flow occurrence information comes from Eden Canyon near gage 1934 (fig. 1, table 2), slightly north of the Walpert Ridge study area. At this location, a debris flow flowed down a channel, across Eden Canyon road, and impacted a house at the base of the valley. According to the homeowner, the flow hit the house between 02:00 and 02:30 on February 3. At gage 1934, none of the rainfall totals for 1-, 6-, 12-, 18-, and 24-hour time periods exceed previously established debris-flow thresholds (table 6). The end times for maximum 1-, 6-, 12-, 18-, and 24-hour rainfall at gage 1934 were 00:00, 01:40, 1:10, 3:00, and 02:40 on February 3, respectively (table 6). The correspondence between the 6- and 24-hour end times and the time that the debris-flow hit the house suggest that the maximum 6- or 24-hour rainfall was the intensity/duration trigger for Eden Canyon debris flow.

APPLICATION OF RESULTS TO HAZARD MAPPING

The results presented in this report show that gradient and topographic curvature (as determined from a 10-m DEM) are the topographic characteristics that can be used to predict the source areas of debris flows in Alameda County. Our data indicate that 94 percent of debris flows initiated from gradients equal or greater than 10° and that debris flow incidence increased as gradient increased. Both divergent and convergent locations are potential debris-flow source areas. At and below about 24∞ debris flows tended to initiate from convergent locations, whereas above 24∞ debris flows tended to initiate from divergent locations. Geologic materials (mapped at a regional scale) and size of upslope contributing area were not good predictors of debris flow source areas. A relative susceptibility ranking based on the number of debris flows/km^2 in each geologic-materials unit does not correlate with the physical properties of these units that would be expected to control susceptibility. This disparity suggests that the susceptibility ranking for geologic materials units is specific to the February storm, and that use of this ranking to predict susceptibility in more general conditions would result in erroneous maps. Additionally, our data indicate that widespread debris flows were triggered by rainfall that was less than existing debris-flow thresholds and that debris flows occurred during and after a 6-hour period of intense rainfall that was preceded by a long period of moderate rainfall.

ACKNOWLEDGMENTS

We thank Bruce Coffland of the NASA Ames Research Center, and Dick Pike and David Howell of the USGS in Menlo Park, California, for furnishing the aerial photographs used for mapping. John Kobar of the National Climatic Data Center gave helpful advice regarding NEXRAD data. Numerous homeowners, as well as Steve Radcliffe of Caltrans, provided information regarding the time of occurrence for debris flows. Andreas Godfrey of the Alameda County Public Works Agency supplied rainfall data from ALERT gages near the study area. Numerous conversations with Sue Cannon and Ray Wilson were helpful. Mark Reid provided data from interviews with homeowners in the study area. Dino Bellugi of the Department of Earth and Planetary Science at Berkeley supplied us with the SHALSTAB equation for total curvature. Steve Ellen and Sue Cannon provided excellent critical reviews of the map report. We are particularly grateful to Margo Johnson for preparing and editing the final map sheets. We appreciate the support of all of these people, but make it clear that any remaining errors are our own.